

Targeting of a Helix-Loop-Helix Transcriptional Regulator by a Short Helical Peptide

Cornelia Roschger^{+, [a]}, Saskia Neukirchen^{+, [a, b]}, Brigitta Elsässer^{, [a]}, Mario Schubert^{, [a]},
Nicole Maeding^{, [c]}, Thomas Verwanger^{, [c]}, Barbara Krammer^{, [c]} and Chiara Cabrele^{*, [a]}

The Id proteins (Id1–4) are cell-cycle regulators that play a key role during development, in cancer and vascular disorders. They contain a conserved helix-loop-helix (HLH) domain that folds into a parallel four-helix bundle upon self- or hetero-association with basic-HLH transcription factors. By using such protein–protein interactions, the Id proteins inhibit cell differentiation and promote cell-cycle progression. Accordingly, their supporting role in cancer has been convincingly demonstrated, which makes these proteins interesting therapeutic targets.

Herein we present a short peptide containing an (i,i+4)-lactam bridge and a hydrophobic (Φ) three-residue motif $\Phi(i)-\Phi(i+3)-\Phi(i+6)$, which adopts a helical conformation in water, shows Id protein binding in the low-micromolar range, penetrates into breast (MCF-7 and T47D) and bladder (T24) cancer cells, accumulates in the nucleus, and decreases cell viability to ~50%. Thus, this cyclopeptide is a promising scaffold for the development of Id protein binders that impair cancer cell viability.

Introduction

The inhibitors of DNA binding and cell differentiation Id1 through Id4 are helix-loop-helix (HLH) transcriptional regulators that play a key role during development, in cancer and vascular disorders.^[1–10] These proteins negatively regulate gene expression mediated by the ubiquitous basic-HLH (bHLH) transcription factors of the E family (E12, E47, Heb and E2-2).^[11,12] Their mode of action is based on the sequestration of the E proteins by interaction of the corresponding HLH domains, which triggers Id/E heterodimerization.^[13] The three-dimensional structures of the homodimeric forms of the HLH domains of Id2 and Id3 (PDB ID: 4AYA for Id2 30–82,^[14] and PDB ID: 2LFH for Id3 29–83)^[15] are both characterized by the presence of a parallel four-helix bundle. In contrast, the monomeric states of the Id proteins are predicted to contain high degree of flexibility,^[16] which seems to be a common feature of eukaryotic transcription factors;^[17] in particular, the HLH domain may undergo folding upon dimerization and oligomerization,^[18–20] whereas the flanking regions remain flexible.^[19–21] However, this does not exclude the latter regions from containing motifs for mo-

lecular recognition: for example, in the case of the Id2 protein it has been shown that the C-terminus contains a nuclear export signal (NES) and a destruction box (D-box) that are recognized by the nuclear export receptor chromosome region maintenance protein 1^[22] and the anaphase-promoting complex, respectively.^[23] In addition, a short N-terminal motif of Id2 has been shown to bind the von-Hippel-Lindau ubiquitin ligase complex, which inhibits ubiquitination of hypoxia inducible factor alpha (HIF α) and thus supports the maintenance of cancer stem cells.^[24] All this supports the fact that Id2 is able to interact with multiple classes of proteins by exploiting different motifs along the sequence.

Based on the significance of the Id proteins as therapeutic targets,^[3,13,25,26] synthetic Id protein binders would be very useful tools to further understand the biology of these proteins as well as to develop Id-protein-directed compounds for diagnostic and therapeutic applications. In this work we explored the possibility to target the HLH region of the Id proteins, which is the most conserved one within the four homologous proteins (Figure 1 a), by using synthetic peptide-based ligands. Previously, medium-sized Id protein binding sequences were identified by phage display based on the Heb HLH domain^[27] or from a randomized combinatorial expression library using yeast and mammalian two-hybrid systems.^[28] We^[29] and others^[30] demonstrated the utility of short linear peptides (Figure 1 b) with intrinsic helix propensity to bind the HLH domain of the Id family and to inhibit proliferation of Id protein expressing cells. Based on these results, we reasoned that the enhancement of the intrinsic helix propensity of a sequence should be of benefit for a better mimicry of interacting helices. In a previous work,^[31] we used the Lys-Asp-(i,i+4)-lactam-bridge constraint to stabilize the helical conformation of octapeptides extracted from the Id HLH domain.^[16] In this

[a] C. Roschger,⁺ S. Neukirchen,⁺ Dr. B. Elsässer, Dr. M. Schubert, Prof. Dr. C. Cabrele
Department of Molecular Biology, University of Salzburg, Billrothstrasse 11, 5020 Salzburg (Austria)
E-mail: chiara.cabrele@sbg.ac.at

[b] S. Neukirchen⁺
Department of Chemistry and Biochemistry, Ruhr-University Bochum, Universitaetsstrasse 150, 44801 Bochum (Germany)

[c] N. Maeding, Dr. T. Verwanger, Prof. Dr. B. Krammer
Department of Molecular Biology, University of Salzburg, Hellbrunnerstrasse 34, 5020 Salzburg (Austria)

[*] These authors contributed equally to this work.

Supporting information and the ORCID identification number(s) for the author(s) of this article can be found under:
 <https://doi.org/10.1002/cmdc.201700305>.

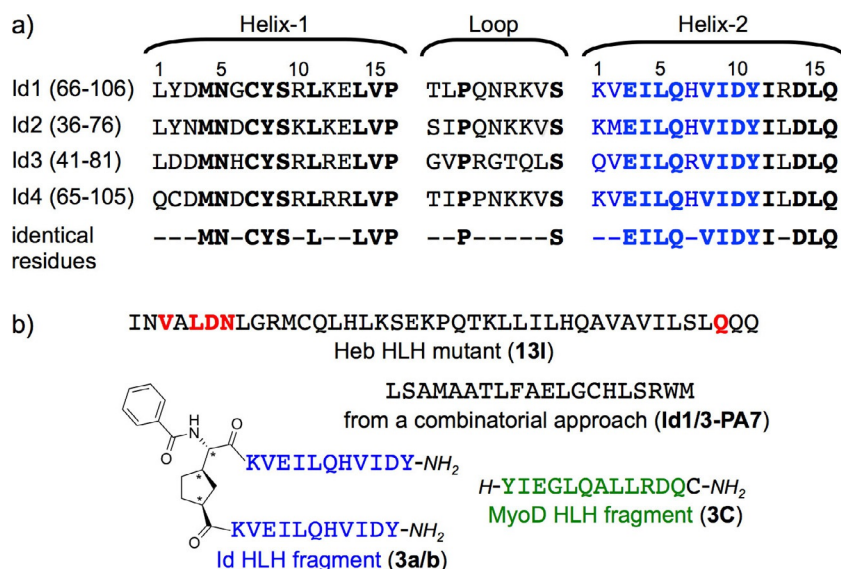


Figure 1. Primary structure of the HLH domain of human Id1-4 and of known peptide-based Id protein binders. a) Sequence alignment of the Id1-4 HLH domains (the fully conserved residues are in bold; the blue-colored sequence represents the part of helix-2 contained in the artificial Id protein binder **3 a/b** shown in panel b, and in the linear peptide **2** described in the section Results and Discussion). b) Amino acid sequences of three artificial Id protein binders (their labels in bold correspond to those used in the original papers): the Heb HLH mutant **13I** (the mutated positions are in red),^[27] the peptide aptamer **Id1/3-PA7**,^[28] the covalent dimer of the Id helix-2 fragment (colored in blue) **3 a/b**,^[29] and the MyoD HLH fragment **3C**.^[30]

work, we present the structural and biological characterization of cyclo-[2,6]-(Ac-VKRLQDLQ-NH₂) (**1**). We used 2D-NMR spectroscopy and molecular dynamics to confirm the helical conformation of **1** in water, which had been suggested previously^[31] by circular dichroism (CD) spectroscopy. Moreover, we evaluated the binding properties of **1** for the Id family by using the Id2 protein as representative member. Cell uptake as well as cell responses upon incubation with the cyclopeptide were performed on breast (MCF-7, T47D) and bladder (T24) cancer cell lines: besides the effect of the cyclopeptide on cell viability, its effects on cell-cycle distribution, cell proliferation and apoptosis were also investigated.

Results and Discussion

We investigated the conformational properties of **1** by 2D-NMR spectroscopy and molecular dynamics (Figure 2 and Supporting Information Figures S2 and S3, and Tables S2, S4 and S5). The resulting structure showed a well-defined helical turn over the cyclized residues, which was stabilized by the backbone H-bonds CO(V1)-HN(L4) (1.98 Å), CO(K2)-HN(D6) (2.68 Å) and CO(R3)-HN(L7) (2.07 Å) (Supporting Information Figure S6).

To see if cyclopeptide **1** was able to mimic a helical motif of the Id HLH fold, we used the crystal structure available for the Id2 HLH domain (PDB ID: 4AYA)^[14] (a solution NMR structure of the Id3 HLH domain is also available,^[15] which is similar to that of the Id2 HLH one, as shown by structure overlap in the Supporting Information Figure S8). We superimposed the hydrophobic three-residue motif V1-L4-L7 of **1** with the hydrophobic (Φ) three-residue motifs $\Phi(i)-\Phi(i+3)-\Phi(i+6)$ present in helix-1 and helix-2 of Id2. We obtained good superposition, with RMSD values ranging from 1.13 Å to 1.38 Å over the C α atoms (Supporting Information Table S8). In all superpositions

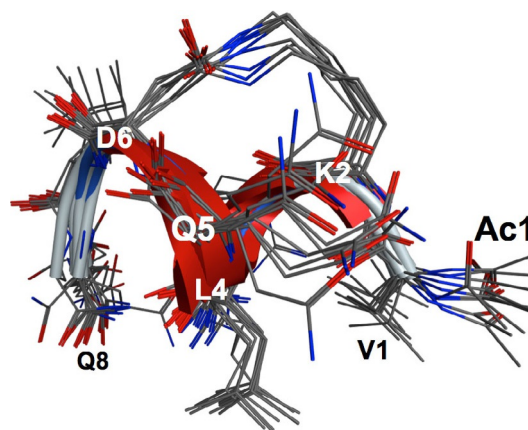


Figure 2. NMR-derived structure of cyclo-[2,6]-(Ac-VKRLQDLQ-NH₂) (**1**). Superposition of the ten lowest energy structures from the molecular dynamics simulation.

the N α -acetyl group of V1 and the side chains of L4 and L7 adopted orientations close to those of the native residues $\Phi(i)$, $\Phi(i+3)$ and $\Phi(i+6)$, respectively (Figure 3 and Supporting Information Figure S9). In particular, superposition of **1** with the helix-2 fragment containing M62, L65 and V68 showed good mimicry of L65 with L4, V68 with L7, and of the SCH₃ group of M62 with the N-terminal acetyl group (Figure 3c).

Further, we investigated whether the helix of **1** would fit in the four-helix bundle in place of the native helix-1 or helix-2. Therefore, for each superposition reported in Figure 3 the corresponding native helix was removed and the structure of the resulting complex was minimized. In all four cases, several hydrophobic and polar interactions were formed, however, the synthetic helix **1** made major contacts to all three other helices

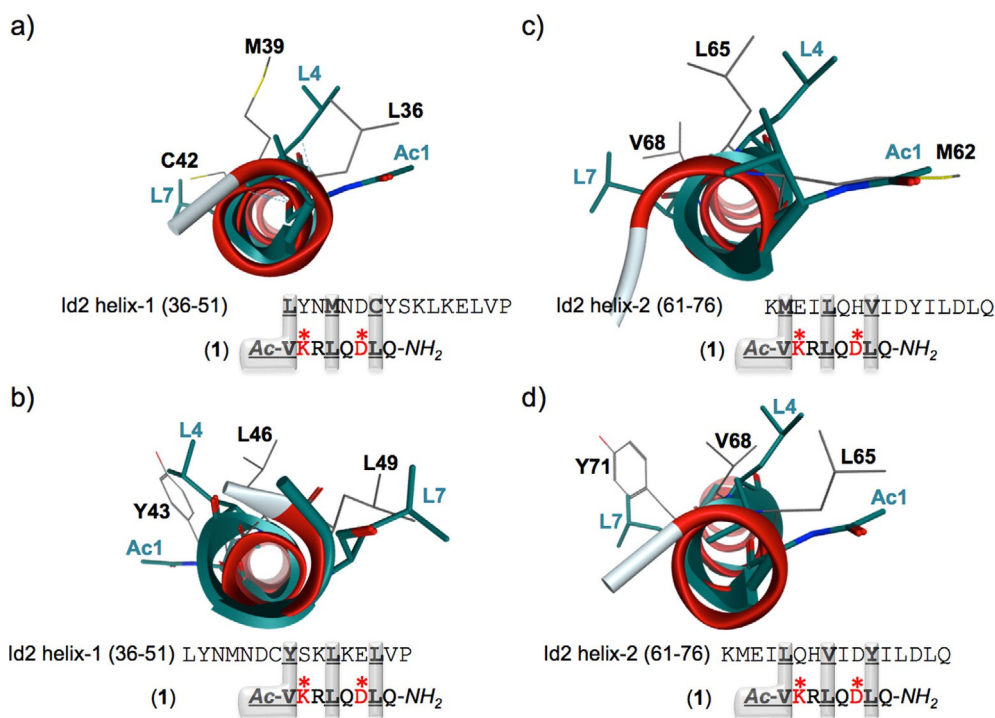


Figure 3. Mimicking hydrophobic patterns of the Id protein helical regions. Comparison of the hydrophobic (Φ) three-residue pattern $\Phi(i) - \Phi(i+3) - \Phi(i+6)$ of **1** with those of Id2 helix-1 (a, b) and helix-2 (c, d) (PDB ID: 4AYA). The hydrophobic three-residue pattern of **1** is colored in teal, those of the helices in the crystal are in grey. The asterisks indicate the presence of the lactam bridge in **1**.

when it replaced the helix-2 three-residue pattern with M62, L65 and V68 (Supporting Information Figure S10c).

Next, we performed peptide–protein binding studies by using Id2 expressed in *E. coli* and an analogue of **1** bearing a tyrosine residue at position nine (**1Y**) as UV-active label to facilitate the measurement of the peptide concentration. The additional C-terminal residue did not affect the helical conformation of **1**, as supported by the superposition of the NMR-derived structures of **1** and **1Y** (Supporting Information Figure S7b). We applied the surface acoustic wave (SAW) biosensor technology^[32] to determine the binding affinity: the protein was covalently immobilized on the self-assembled monolayer on a gold chip, and the binding of **1Y** was monitored by measuring the change of the SAW phase.

The fitting of the binding isotherm was performed with the Hill equation, to extrapolate the $K_{0.5}$ value and the Hill coefficient: a $K_{0.5}$ value of $\approx 2 \mu\text{M}$ and a Hill coefficient of ≈ 2 for the binding between **1Y** and Id2 were obtained (Figure 4). We also measured the binding properties of the linear Id helix-2 fragment that was previously used to target the Id proteins^[29,30] (Ac-KVEILQHVIDY-NH₂, **2**). This fragment contains two potential hydrophobic three-residue patterns of type $\Phi(i) - \Phi(i+3) - \Phi(i+6)$: V62-L65-V68, or L65-V68-Y71. The affinity of the linear peptide **2** to Id2 was about two times lower than that of **1Y** (Figure 4). Interestingly, the Hill coefficient was ≈ 2 for both ligands, which would infer that a cooperative binding of at least two sites might occur. Indeed, this cannot be excluded, as the Id HLH domain consists of two helix-prone fragments with strong tendency to form a four-helix bundle upon dimerization, as shown in the crystal and solution-NMR structures of

the HLH domains of Id2^[14] and Id3,^[15] respectively. We also observed that the binding of the peptide to the immobilized protein was coupled to decreased viscoelasticity of the self-assembled monolayer covering the gold chip, which would suggest increased flexibility of the protein–peptide complex with respect to the unbound protein (Supporting Information Figures S11 and S12). One explanation for this observation might be a decrease in self-association of the protein and/or a compensation of entropy loss upon peptide binding by enhanced dynamics of some protein backbone regions, a binding mechanism (unfolding-upon-binding) that has been recently suggest-

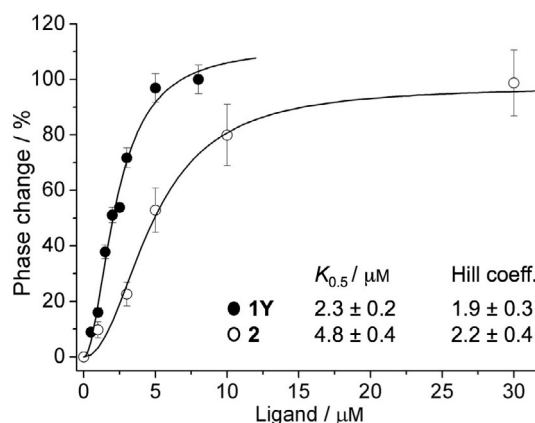


Figure 4. Binding of the lactam-bridged nonapeptide **1Y** and of the linear undecapeptide **2** to the Id2 protein. The latter was immobilized on the self-assembled monolayer of a gold chip (changes of the phase of a surface acoustic wave upon binding were used as response).

ed for the binding of heparin to the intrinsically disordered cytokine osteopontin.^[33] However, the elucidation of the mode of interaction of the peptide binders with the protein will require detailed structural investigation.

We tested the ability of **1Y** to affect the viability of various cancer cell types, whose progression to highly invasive and metastatic stages has been associated with dysregulation of the Id protein family members.^[4,10] For this purpose, we used two breast adenocarcinoma cell lines (MCF-7 and T47D) and the urinary bladder carcinoma cell line (T24).^[34–39] As a control for non-cancer cells, and to exclude general cytotoxic effects of the peptide, we used primary human lung fibroblasts that contain very low Id protein levels relative to the investigated cancer cell lines. The cells were incubated with increasing concentrations of **1Y** (up to 1 mM) for 24 h and the viable cells were then detected by the thiazolyl blue tetrazolium bromide (MTT) assay.^[40] In contrast to the primary human lung fibroblasts that did not show relevant changes in viability over the investigated peptide concentration range (Supporting Information Figure S20), the three cancer cell lines gave dose-response curves with a minimum of cell viability close to 50%, and an inflection point ranging from 4 μM to 47 μM (Figure 5). In comparison with the linear Id helix-2 fragment **2**, cyclopeptide **1Y** was by trend more efficacious, particularly with respect to the breast cancer cell line T47D (Figure 5b). It has been reported that the two breast cancer cell lines MCF-7 and T47D may show different sensitivity toward anticancer drugs, which is likely to reflect a distinct proteomic profile^[41] and the activation of different apoptotic pathways: for example, different caspases (i.e., caspase-3/-7 in T47D cells, and caspase-6 in MCF-7 cells, the latter being caspase-3 negative)^[42] seem to be activated.^[43] Sensitivity toward doxorubicin has been reported to be higher for the T47D cells than for the MCF-7 cells.^[44] Moreover, MCF-7 and T47D cells have shown different responses toward the microtubule-depolymerizing agents nocodazole, vincristine and colchicine, with much stronger induction of a mitotic arrest in the MCF-7 cells than in the T47D cells, and with p21 increase in the T47D cells but not in the MCF-7 cells.^[45] It will be interesting to investigate the effect of **1Y** on the two breast cancer cell lines and also on the urinary bladder cancer cell line T24 at the transcriptomic and proteomic levels in the near future.

The observation that **1Y** and **2** partially (rather than fully) suppressed cell viability is in agreement with previous work, where peptide-based molecules targeting the Id proteins, like the Heb HLH mutant^[46] **13I** and the covalent dimer of the Id HLH fragment **3a/b** shown in Figure 1b,^[29] or antisense oligonucleotides against Id1-3 mRNAs^[47,48] were applied to inhibit the proliferation of different cell types. However, to exclude that this behavior might arise from poor cell permeability toward the peptides, we monitored the time-dependent cell uptake of fluorescent analogues of **1Y** and **2** containing 5(6)-carboxyfluorescein- β -alanine in place of the N-terminal acetyl group (**FAM-1Y** and **FAM-2**). Both peptides (10 μM) accumulated in the cell nucleus already after 8 h incubation at 37 $^{\circ}\text{C}$ (Figure 6). We also investigated shorter and longer incubation times: no significant differences were detected on the cells

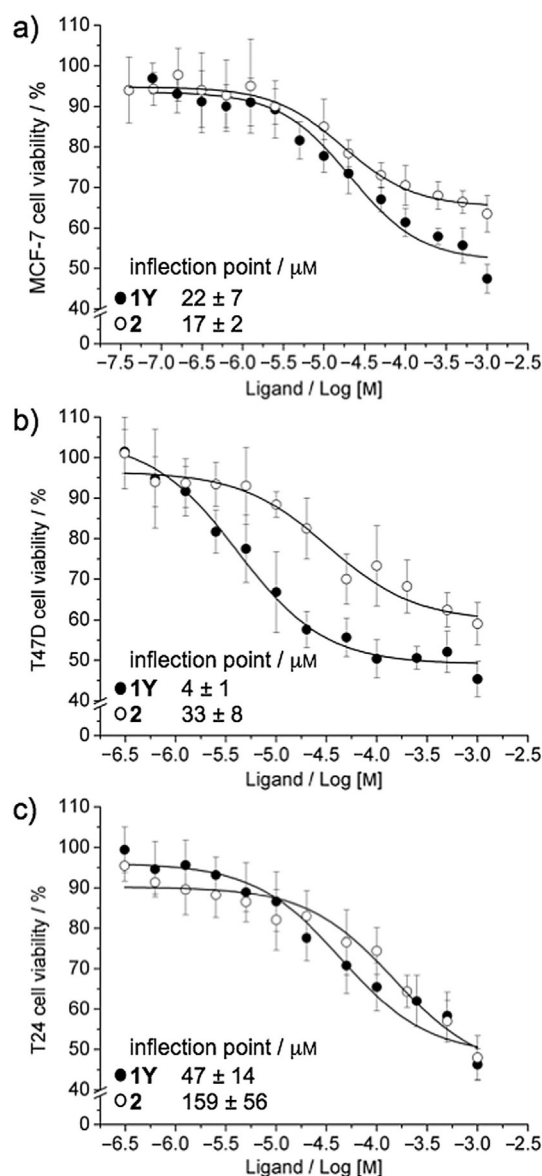


Figure 5. Effect of **1Y** and **2** on cancer cell viability. Viability of a) MCF-7, b) T47D, and c) T24 cells treated with cyclopeptide **1Y** or the linear Id helix-2 fragment **2** for 24 h was determined by the MTT assay. The effect of **1Y** and **2** on the viability of the primary human lung fibroblasts is shown in Figure S20 of the Supporting Information. The graphs represent the mean value \pm SD of at least three independent experiments. Peptide stability studies in the cell culture medium containing 5% fetal bovine serum, in human blood serum and in the presence of trypsin are reported in the Supporting Information (Figures S13 and S14).

treated for 12 h, 16 h, and 24 h (Supporting Information Figures S15–17); importantly, necrotic cells were not observed, not even at 24 h (Supporting Information Figure S24), which excludes loss of cell membrane integrity. Contrarily to **FAM-1Y**, **FAM-2** was found in the majority of the MCF-7 cells already after 4 h incubation (Supporting Information Figure S18a). However, neither **FAM-1Y** nor **FAM-2** were found in the cells upon incubation at 4 $^{\circ}\text{C}$ for 8 h (Supporting Information Figure S18c), which suggests that an energy-dependent, endocytosis-mediated transport mechanism^[49,50] might play a role.

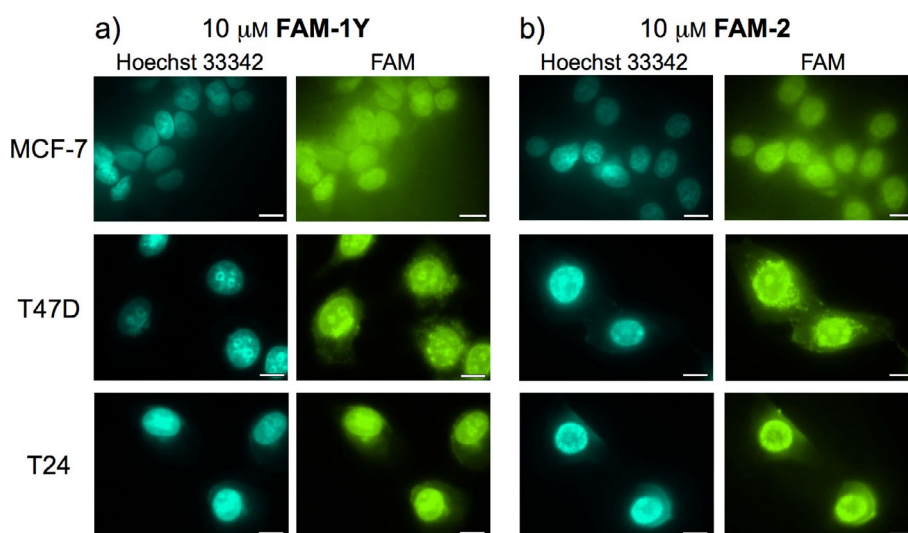


Figure 6. Uptake of the fluorescence-labeled peptides a) **FAM-1Y** and b) **FAM-2** into MCF-7, T47D, and T24 cells. Fluorescence microscopy images were taken after 8 h incubation with each peptide at 10 μM . Nuclei were stained with the Hoechst 33342 nucleic acid stain and are visible in cyan (scale bar: 10 μm).

However, an energy-independent uptake mechanism based on direct penetration cannot be excluded to take place at peptide concentrations higher than 10 μM , which was the one used in this cellular uptake experiment. Moreover, besides the peptide concentration,^[51] several other aspects, like the incubation time,^[52] the selective chemical inhibition of endocytotic pathways,^[52,53] the subcellular peptide distribution and the Id protein/peptide co-localization, will require further investigation for a detailed characterization of the cellular uptake of **1Y** and **2**.

Further, we investigated the effect of **1Y** and **2** (100 μM) on the cell cycle after 24 h treatment. We found that **2** increased the amount of small DNA fragments exhibiting fluorescence of at least two orders of magnitude lower than that of the G_0/G_1 phase (events at $<G_0/G_1$) (Figure 7a–c and Supporting Information Figures S21–23), which indicates cell death induction. Cyclopeptide **1Y** behaved similarly with the T47D and T24 cells, but not with the MCF-7 cells, whose fraction of small DNA fragments was similar to that of the control (Figure 7a). This was surprising, as the MTT assay had shown a significant decrease in MCF-7 cell viability upon **1Y** treatment (Figure 5a). To see whether **1Y** was inducing cell death at shorter incubation times, we measured the cell cycle of MCF-7 cells after 8 h and 18 h treatment with **1Y**. The results showed no significant changes of the respective cell-cycle phases G_0/G_1 , S and G_2/M (Supporting Information Table S9), but an increase in the weakly fluorescing DNA fragments from 7% of total events at $<G_0/G_1$ in the control to 19% and 14% of total events at $<G_0/G_1$ after 8 h and 18 h treatment, respectively, which is indicative of cell death induction (Figure 7a).

The temporarily induced MCF-7 cell death was caused by apoptotic and not by necrotic processes, as shown by the propidium iodide/3,3'-dihexyloxycarbocyanine iodide (PI/DiOC₆) assay^[54] (Figure 8). We found, however, less than 20% apoptotic cells after 8 h and none after 24 h (Supporting Information Figure S24), which is divergent from the decrease in cell viability

of ~40% observed by the MTT assay in the time frame between 8 h and 24 h (Supporting Information Figure S19) when the same peptide concentration was applied (Figure 5a).

To search for the origin of this discrepancy, we investigated the effect of **1Y** on the proliferative capacity of this cell line. For this purpose, we applied the CFSE (carboxyfluorescein diacetate succinimidyl ester) proliferation assay^[55] that determines cell division based on the dilution of the CFSE dye with each proliferation cycle. MCF-7 cells treated with cyclopeptide **1Y** for 24 h proliferated less than the untreated control cells (Figure 9). Altogether, the viability (MTT), apoptosis/necrosis ($<G_0/G_1$ and PI/DiOC₆) and proliferation (CFSE) assays on the MCF-7 cells treated with **1Y** suggest that the cellular response to **1Y** consists of the activation of apoptotic processes as well as of pathways that influence the cell cycle. In fact, the Id proteins are involved in cell-cycle control, particularly by inducing the G_0 -S transition,^[47,56–58] whereas their inhibition by antisense oligonucleotides was shown to delay the re-entry of arrested cells into the cell cycle upon stimulation with serum or growth factors.^[47,57] Although the cell-cycle analysis does not reveal any clear arrest (Supporting Information Table S9), we cannot exclude that the negative effect of **1Y** on cell proliferation might indeed reflect a subtle cell-cycle arrest. Further investigation based on the use of different cell-cycle indicators, transcriptomic and/or proteomic approaches will be necessary to identify those pathways that may be influenced by **1Y** and mediate the effect of the latter on the MCF-7 cell growth.

Conclusions

We found a useful cyclopeptide scaffold to target the Id proteins in cancer cells and to impair their viability by inducing cell death and/or by decreasing cell proliferation. The performance of the cyclic nine-residue scaffold (**1Y**) in Id protein binding and inhibition was slightly superior to that of the linear 11-residue peptide (**2**). Moreover, the former offers the

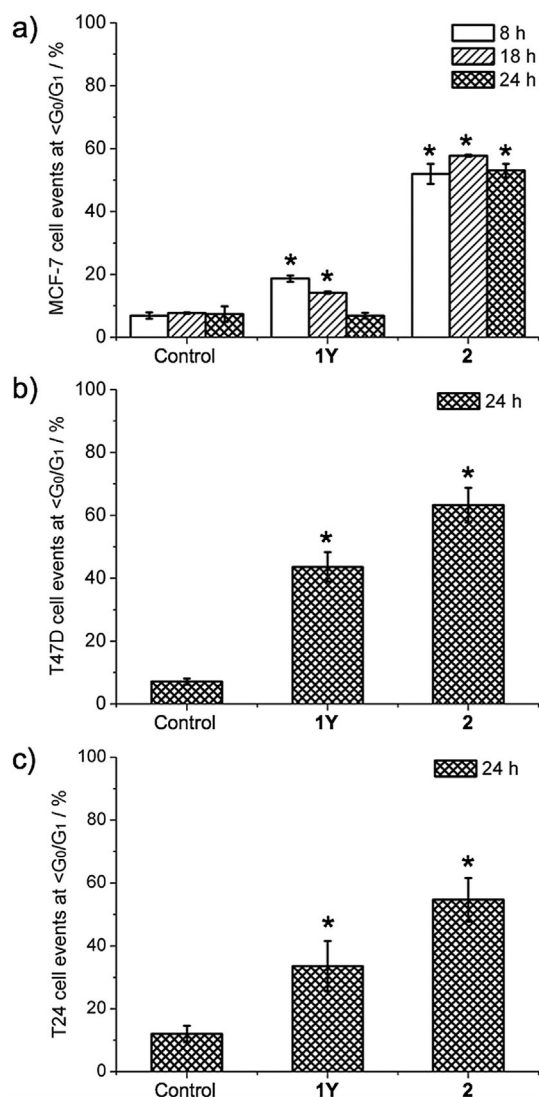


Figure 7. Peptide-induced cell death, as indicated by the detection of small DNA fragments (events at $<G_0/G_1$). a) MCF-7, b) T47D, and c) T24 cells were treated with $100\ \mu\text{M}$ cyclopeptide 1Y or linear peptide 2 for the indicated times and analyzed by flow cytometry. The graphs represent the mean value \pm SD of at least three independent experiments ($*p \leq 0.01$ with respect to control).

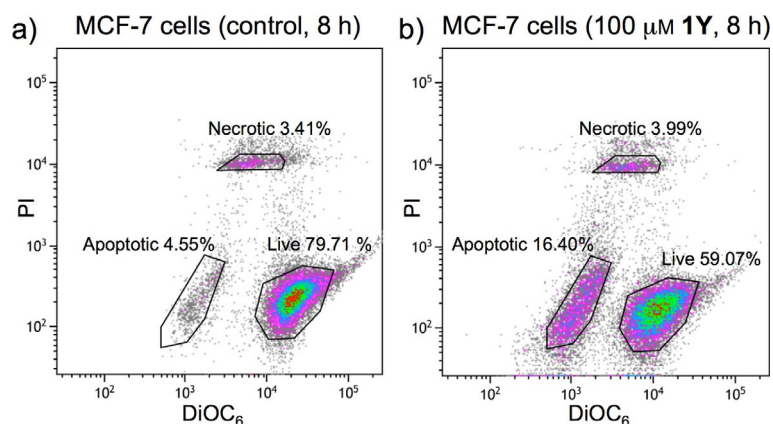


Figure 8. Cytotoxic effect of 1Y on MCF-7 cells. a) Untreated and b) treated ($100\ \mu\text{M}$ 1Y, 8 h) cells were exposed to the dye DiOC₆ and the DNA/RNA intercalating dye propidium iodide (PI) to detect apoptotic cells (reduced mitochondrial membrane potential, low DiOC₆ staining) and necrotic cells (no plasma membrane integrity, high PI staining), respectively.

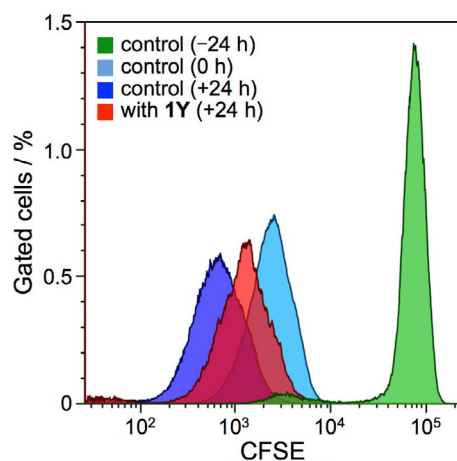


Figure 9. Effect of cyclopeptide 1Y on the proliferation of MCF-7 cells. The latter were stained with $10\ \mu\text{M}$ CFSE. Staining control was measured immediately (green) after CFSE addition and after 24 h (light blue). The cells were incubated for another 24 h without (dark blue) and with (red) $100\ \mu\text{M}$ 1Y.

possibility to better control the three-dimensional structure of the binding peptide, which will facilitate the design of Id protein inhibitors with enhanced protein-binding affinity in the future, e.g., by varying the hydrophobic three-residue motif $\Phi(i)-\Phi(i+3)-\Phi(i+6)$, by using alternative tethered peptides^[59–61] or foldamers.^[62,63]

Experimental Section

The detailed description of all materials, methods, procedures for peptide and protein preparation, peptide characterization by HPLC, MS and NMR spectroscopy, distance-constrained molecular modeling, binding studies by SAW biosensor technology, peptide stability in human blood serum and in the presence of trypsin, cancer cell and primary human lung fibroblast viability assays, cell uptake at $4\ ^\circ\text{C}$ and $37\ ^\circ\text{C}$, cell cycle and proliferation analysis, apoptosis/necrosis assay, as well as additional figures (including images of cell uptake, histograms and density plots of the FACS data) and tables are provided in the Supporting Information.

Acknowledgements

C.C. acknowledges the Land Salzburg for funding. B.E. thanks the Austrian Science Fund (FWF) for the Lise-Meitner Grant (no. M1901). The authors also thank Sabine Markovic-Ullrich and Vesna Stanojlovic for their support with the HPLC and MS measurements.

Conflict of interest

The authors declare no conflict of interest.

Keywords: cell growth inhibition · cyclopeptides · Id proteins · peptide–protein interactions

- [1] D. Patel, D. J. Morton, J. Carey, M. C. Havrda, J. Chaudhary, *Biochim. Biophys. Acta Rev. Cancer* **2015**, *1855*, 92–103.
- [2] W. S. Teo, R. Nair, A. Swarbrick, *Breast Cancer Res.* **2014**, *16*, 305.
- [3] R. Nair, W. S. Teo, V. Mittal, A. Swarbrick, *Mol. Ther.* **2014**, *22*, 1407–1415.
- [4] A. Lasorella, R. Benezra, A. Iavarone, *Nat. Rev. Cancer* **2014**, *14*, 77–91.
- [5] M. T. Ling, X. Wang, X. Zhang, Y. C. Wong, *Differentiation* **2006**, *74*, 481–487.
- [6] A. Iavarone, A. Lasorella, *Trends Mol. Med.* **2006**, *12*, 588–594.
- [7] S. Forrest, C. McNamara, *Arterioscler. Thromb. Vasc. Biol.* **2004**, *24*, 2014–2020.
- [8] M. B. Ruzinova, R. Benezra, *Trends Cell Biol.* **2003**, *13*, 410–418.
- [9] A. Lasorella, T. Uo, A. Iavarone, *Oncogene* **2001**, *20*, 8326–8333.
- [10] C. Roschger, C. Cabrele, *Cell Commun. Signaling* **2017**, *15*, 7.
- [11] K. Langlands, X. Yin, G. Anand, E. V. Prochownik, *J. Biol. Chem.* **1997**, *272*, 19785–19793.
- [12] P. J. O'Toole, T. Inoue, L. Emerson, I. E. Morrison, A. R. Mackie, R. J. Cherry, J. D. Norton, *J. Biol. Chem.* **2003**, *278*, 45770–45776.
- [13] W. Garland, R. Benezra, J. Chaudhary, *Annu. Rep. Med. Chem.* **2013**, *48*, 227–245.
- [14] M. V. Wong, S. Jiang, P. Palasingam, P. R. Kolatkar, *PLoS One* **2012**, *7*, e48591.
- [15] A. Eletsky, D. Wang, E. Kohan, H. Janjua, T. B. Acton, R. Xiao, J. K. Everett, G. T. Montelione, T. Szyperski, **2011**, DOI: <https://doi.org/10.2210/pdb2ffh/pdb>.
- [16] M. Beisswenger, C. Cabrele, *Biochim. Biophys. Acta Proteins Proteomics* **2014**, *1844*, 1675–1683.
- [17] X. Guo, M. L. Bulyk, A. J. Hartemink, *Pacific Sympos. Biocomput.* **2012**, *104*–115.
- [18] R. Fairman, R. K. Beran-Steed, S. J. Anthony-Cahill, J. D. Lear, W. F. Stafford III, W. F. DeGrado, P. A. Benfield, S. L. Brenner, *Proc. Natl. Acad. Sci. USA* **1993**, *90*, 10429–10433.
- [19] S. D. Kiewitz, C. Cabrele, *Biopolymers* **2005**, *80*, 762–774.
- [20] J. Svobodová, C. Cabrele, *ChemBioChem* **2006**, *7*, 1164–1168.
- [21] N. Colombo, C. Cabrele, *J. Pept. Sci.* **2006**, *12*, 550–558.
- [22] H. Kurooka, Y. Yokota, *J. Biol. Chem.* **2005**, *280*, 4313–4320.
- [23] A. Lasorella, J. Stegmuller, D. Guardavaccaro, G. Liu, M. S. Carro, G. Rothschild, L. de la Torre-Ubieta, M. Pagano, A. Bonni, A. Iavarone, *Nature* **2006**, *442*, 471–474.
- [24] S. B. Lee, V. Frattini, M. Bansal, A. M. Castano, D. Sherman, K. Hutchinson, J. N. Bruce, A. Califano, G. Liu, T. Cardozo, A. Iavarone, A. Lasorella, *Nature* **2016**, *529*, 172–177.
- [25] S. Fong, R. J. Debs, P. Y. Desprez, *Trends Mol. Med.* **2004**, *10*, 387–392.
- [26] R. Benezra, *Biochim. Biophys. Acta Rev. Cancer* **2001**, *1551*, F39–F47.
- [27] R. Ciarapica, J. Rosati, G. Cesareni, S. Nasi, *J. Biol. Chem.* **2003**, *278*, 12182–12190.
- [28] D. S. Mern, K. Hoppe-Seyler, F. Hoppe-Seyler, J. Hasskarl, B. Burwinkel, *Breast Cancer Res. Treat.* **2010**, *124*, 623–633.
- [29] S. Pellegrino, N. Ferri, N. Colombo, E. Cremona, A. Corsini, R. Fanelli, M. L. Gelmi, C. Cabrele, *Bioorg. Med. Chem. Lett.* **2009**, *19*, 6298–6302.
- [30] C. H. Chen, S. C. Kuo, L. J. Huang, M. H. Hsu, F. D. Lung, *J. Pept. Sci.* **2010**, *16*, 231–241.
- [31] S. Neukirchen, V. Krieger, C. Roschger, M. Schubert, B. Elsässer, C. Cabrele, *J. Pept. Sci.* **2017**, *23*, 587–596.
- [32] N. Bracke, S. Barhdadi, E. Wynendaele, B. Gevaert, M. D'Hondt, B. De Spiegeleer, *Sens. Actuators B* **2015**, *210*, 103–112.
- [33] D. Kurzbach, T. C. Schwarz, G. Platzer, S. Hoffer, D. Hinderberger, R. Konrat, *Angew. Chem. Int. Ed.* **2014**, *53*, 3840–3843; *Angew. Chem.* **2014**, *126*, 3919–3922.
- [34] H. Kim, H. Chung, H. J. Kim, J. Y. Lee, M. Y. Oh, Y. Kim, G. Kong, *Breast Cancer Res. Treat.* **2008**, *112*, 287–296.
- [35] Y. Ding, G. Wang, M. T. Ling, Y. C. Wong, X. Li, Y. Na, X. Zhang, C. W. Chua, X. Wang, D. Xin, *Int. J. Oncol.* **2006**, *28*, 847–854.
- [36] S. Fong, Y. Itahana, T. Sumida, J. Singh, J. P. Coppe, Y. Liu, P. C. Richards, J. L. Bennington, N. M. Lee, R. J. Debs, P. Y. Desprez, *Proc. Natl. Acad. Sci. USA* **2003**, *100*, 13543–13548.
- [37] H. Hu, H. Y. Han, Y. L. Wang, X. P. Zhang, C. W. Chua, Y. C. Wong, X. F. Wang, M. T. Ling, K. X. Xu, *Oncol. Rep.* **2009**, *21*, 1053–1059.
- [38] C. Q. Lin, J. Singh, K. Murata, Y. Itahana, S. Parrinello, S. H. Liang, C. E. Gillett, J. Campisi, P. Y. Desprez, *Cancer Res.* **2000**, *60*, 1332–1340.
- [39] D.-H. Shin, J.-H. Park, J.-Y. Lee, H.-Y. Won, K.-S. Jang, K.-W. Min, S.-H. Jang, J.-K. Woo, S. H. Oh, G. Kong, *Oncotarget* **2015**, *6*, 17276–17290.
- [40] T. Mosmann, *J. Immunol. Methods* **1983**, *65*, 55–63.
- [41] J. A. Aka, S. X. Lin, *PLoS One* **2012**, *7*, e31532.
- [42] R. U. Jänicke, *Breast Cancer Res. Treat.* **2009**, *117*, 219–221.
- [43] L. M. Mooney, K. A. Al-Sakkaf, B. L. Brown, P. R. Dobson, *Br. J. Cancer* **2002**, *87*, 909–917.
- [44] R. A. Susidarti, R. I. Jenie, M. Ikawati, D. D. P. Putri, E. Meiyanto, *J. Appl. Pharm. Sci.* **2014**, *4*, 89–97.
- [45] A. L. Blajeski, V. A. Phan, T. J. Kottke, S. H. Kaufmann, *J. Clin. Invest.* **2002**, *110*, 91–99.
- [46] R. Ciarapica, D. Annibali, L. Raimondi, M. Savino, S. Nasi, R. Rota, *Oncogene* **2009**, *28*, 1881–1891.
- [47] M. V. Barone, R. Pepperkok, F. A. Peverali, L. Philipson, *Proc. Natl. Acad. Sci. USA* **1994**, *91*, 4985–4988.
- [48] E. Henke, J. Perk, J. Vider, P. de Candia, Y. Chin, D. B. Solit, V. Ponomarev, L. Categni, K. Manova, N. Rosen, R. Benezra, *Nat. Biotechnol.* **2008**, *26*, 91–100.
- [49] Z. Guo, H. Peng, J. Kang, D. Sun, *Biomed. Rep.* **2016**, *4*, 528–534.
- [50] N. J. Yang, M. J. Hinner, *Methods Mol. Biol.* **2015**, *1266*, 29–53.
- [51] G. Tünnemann, G. Ter-Avetisyan, R. M. Martin, M. Stöckl, A. Herrmann, M. C. Cardoso, *J. Pept. Sci.* **2008**, *14*, 469–476.
- [52] H. Yamashita, T. Kato, M. Oba, T. Misawa, T. Hattori, N. Ohoka, M. Tanaka, M. Naito, M. Kurihara, Y. Demizu, *Sci. Rep.* **2016**, *6*, 33003.
- [53] M. Mano, C. Teodosio, A. Paiva, S. Simoes, M. C. P. de Lima, *Biochem. J.* **2005**, *390*, 603–612.
- [54] H. M. Korchak, A. M. Rich, C. Wilkenfeld, L. E. Rutherford, G. Weissmann, *Biochem. Biophys. Res. Commun.* **1982**, *108*, 1495–1501.
- [55] X. Q. Wang, X. M. Duan, L. H. Liu, Y. Q. Fang, Y. Tan, *Acta Biochim. Biophys. Sin.* **2005**, *37*, 379–385.
- [56] B. A. Christy, L. K. Sanders, L. F. Lau, N. G. Copeland, N. A. Jenkins, D. Nathans, *Proc. Natl. Acad. Sci. USA* **1991**, *88*, 1815–1819.
- [57] E. Hara, T. Yamaguchi, H. Nojima, T. Ide, J. Campisi, H. Okayama, K. Oda, *J. Biol. Chem.* **1994**, *269*, 2139–2145.
- [58] R. W. Deed, S. M. Bianchi, G. T. Atherton, D. Johnston, M. Santibanez-Koref, J. J. Murphy, J. D. Norton, *Oncogene* **1993**, *8*, 599–607.
- [59] K. Hu, H. Geng, Q. Zhang, Q. Liu, M. Xie, C. Sun, W. Li, H. Lin, F. Jiang, T. Wang, Y. D. Wu, Z. Li, *Angew. Chem. Int. Ed.* **2016**, *55*, 8013–8017; *Angew. Chem.* **2016**, *128*, 8145–8149.
- [60] J. Li, Y. Tian, D. Wang, Y. Wu, X. Ye, Z. Li, *Bioorg. Med. Chem.* **2017**, *25*, 1756–1761.
- [61] H. Lin, Y. Jiang, Q. Zhang, K. Hu, Z. Li, *Chem. Commun.* **2016**, *52*, 10389–10391.
- [62] C. Cabrele, T. A. Martinek, O. Reiser, L. Berlicki, *J. Med. Chem.* **2014**, *57*, 9718–9739.
- [63] R. Gopalakrishnan, A. I. Frolov, L. Knerr, W. J. Drury III, E. Valeur, *J. Med. Chem.* **2016**, *59*, 9599–9621.

Manuscript received: May 19, 2017

Revised manuscript received: July 17, 2017

Accepted manuscript online: July 25, 2017

Version of record online: September 5, 2017